EFFECT OF ATAXIA-TELANGIECTASIA MUTATED (ATM) AND CELL CYCLE

STAGE ON TELOMERE OVERHANG MAINTENANCE

A THESIS

SUBMITTED IN PARTIAL FULFILLMENT OF THE REQUIREMENTS FOR THE

DEGREE OF MASTER OF SCIENCE

IN THE GRADUATE SCHOOL OF THE

TEXAS WOMAN'S UNIVERSITY

COLLEGE OF ARTS AND SCIENCES

BY

AMRUTA BHUSARI, M.S.

DENTON, TEXAS

DECEMBER 2008

TEXAS WOMAN'S UNIVERSITY
DENTON, TEXAS

August 28, 2008

To the Dean of the Graduate School:

I am submitting herewith a thesis written by Amruta Bhusari entitled "Effect Of Ataxia-Telangiectasia Mutated (ATM) And Cell Cycle Stage On Telomere Overhang Maintenance." I have examined this thesis for form and content and recommend that it be accepted in partial fulfillment of the requirements for the degree of Master of Science with a major in Biology.
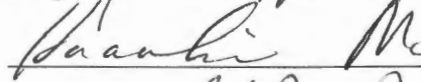
_____
Weihang Chai, Ph.D., Major Professor

We have read this thesis and recommend its acceptance:

_____

_____

_____
Department Chair

Accepted:

_____
Dean of the Graduate School

DEDICATION

To my husband, Satyajit, thank you for your patience and love.

ACKNOWLEDGMENTS

ABSTRACT

AMRUTA BHUSARI

EFFECT OF ATAXIA-TELANGIECTASIA MUTATED (ATM) AND CELL CYCLE
STAGE ON TELOMERE OVERHANG MAINTENANCE

DECEMBER 2008

Telomeres, the physical ends of chromosomes, are indispensable for maintaining genomic stability. Telomeres end in 3′ single stranded G-overhangs. The 3′ overhang is a site where telomerase binds and extends short telomeres. The overhang also participates in the formation of t-loop that protects telomere ends from being recognized as damaged sites. Thus, studying the maintenance of telomere overhangs has become an important aspect of telomere biology. The Ataxia-Telangiectasia Mutated (ATM) protein, encoded by the ATM gene, belongs to the phosphatidyl inositol 3-kinase (PI3K) like kinase (PI3KK) family of proteins. It plays a major role in DNA damage repair and cell cycle regulation. The function of ATM at human telomeres is unclear. In this study, the effect of ATM kinase inhibition on the telomere G-overhang and also the regulation of telomere overhang were studied. This enabled us to understand the particular phase in which the overhang is generated. By telomere overhang protection assay I found that ATM kinase inhibition does not have any effect on the size of telomere overhang length. Also, the generation of telomere overhang is cell cycle stage specific and is independent of telomerase activity. Understanding the mechanism of G-overhang generation in human cells will ultimately help in finding solutions to curb premature aging and cancer.

TABLE OF CONTENTS

LIST OF FIGURES

CHAPTER I

INTRODUCTION

Eukaryotic chromosomes end in a special nucleoprotein complex called telomeres. Telomeres were first discovered by Herman J. Muller while carrying out experiments on *Drosophila*. He found out that each chromosome had to be sealed at both ends by a specialized structure and that this structure was necessary for maintaining chromosome stability. Similarly, studies carried out by Barbara McClintock on maize also showed that without these end caps chromosome-chromosome fusions occurred that threatened the viability of the cell (4). Without telomeres, at the end of every cell division the cell would have lost a lot of important genetic information due to the "end-replication problem" of linear chromosome DNA. The term "end-replication problem" was coined by James Watson (29). DNA polymerases, the chief enzyme involved in the replication of DNA, synthesize DNA in $5' \rightarrow 3'$ direction and require an RNA primer for synthesis. DNA polymerases can thus synthesize the leading strand until the end. However, on the lagging strand the replication machinery is not able to fully synthesize the strand to the end and results in a loss of sequence equal to the length of an RNA primer after each round of replication. Another scientist, Alexy Olovnikov, suggested that the end replication problem was the main reason behind telomere shortening and that with subsequent rounds of replication it could lead to replicative senescence (28).

Telomeres are composed of repetitive G-rich DNA sequences (31) that end with single-stranded 3′ G-rich overhangs (22). The length of telomeres varies in different organisms. Studies carried out by scientists Kipling and Cooke (37) and Makarov and colleagues (27) showed that rats and certain strains of mice have the longest telomeres, up to 150 kb. Humans have up to 10-15 kb of telomeres at birth, which shorten with every cell division (33, 34, 35, 36). Telomere length in yeasts was found out to be about 300 bp (38).

While the majority of telomere DNA is double-stranded, the 3' end of telomere on G-rich strand is single-stranded. The single-stranded telomeric G-rich overhang has a lot of importance since it is the site where telomerase binds to and elongates the telomeres. Griffith, et al. (20) showed that the overhang can be folded to form a lariat-like structure called the t-loop (Figure 1) that helps in the protection of chromosome ends from being recognized as DNA double strand breaks by the DNA damage repair proteins.

Telomerase, a reverse transcriptase that adds the telomeric repeats to the 3′ end of short telomeres, was first discovered in *Tetrahymena* (30). Telomerase has two subunits in human cells: the RNA component called hTR that acts as a template during the elongation of telomeres; and the catalytic component called hTERT that adds the telomeric repetitive sequences at telomere ends. Telomerase is usually inactive in normal somatic cells. However, in about 80% of cancer cell lines, telomerase is activated to maintain telomeres (39).
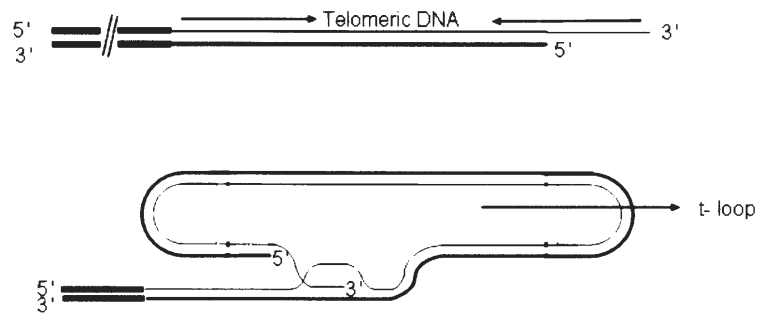
Figure 1. Formation of t-loop. The single-stranded G-rich overhang invades the double-stranded telomeric DNA and forms a loop like structure called the t-loop. This process occurs with the help of telomere binding proteins.

Shelterin

There are proteins that play an important role in the maintenance of telomere. These proteins form a complex called shelterin at the telomeres (9). The shelterin complex consists of six proteins: TRF1, TRF2, POT1, TPP1, TIN2 and Rap1. Telomere repeat binding factor 1 and 2 (TRF1 and TRF2) are DNA double-stranded binding proteins. Protection of telomere 1 (POT1) binds to the single-stranded 3′ overhang of telomeres. TPP1 forms a heterodimer with POT1. TPP1 and POT1 interact with TRF1 and TRF2 through the interaction of TPP1 with another protein called TIN2 (12). The function of Rap1 is not clear but it is thought that it interacts with other proteins RIF1 and RIF2 that brings telomeres to accessible state (41). These proteins (shelterin) control the access of various DNA damage response (DDR) proteins and regulate telomerase activity

3

at telomeres. With the functional loss of any one of these proteins, the telomere ends can be read as double-stranded breaks and acted upon by the DNA double-stranded break repair proteins.

DNA Damage Response

The DDR pathways respond to DNA damage and lead to DNA repair, triggering of apoptotic pathway and checkpoint activity. The DDR begins with the recruitment of the primary sensor protein of DNA damage, the Mre11-Rad50-Nbs1 (MRN) complex at the damaged site. With the recruitment of this complex, a number of downstream effects are seen (16). One of these effects is the activation of the kinase protein Ataxia-telangiectasia mutated (ATM) which is chiefly involved in responding to DNA damage, cell cycle regulation and in the maintenance of genomic stability (15). ATM is a 370kDa protein mainly found in the nucleus. It belongs to the family of phosphatidyl inositol 3-kinase (PI3K) like kinase (PI3KK) proteins. It is a serine-threonine kinase. In addition to the PI3K-like domain at the C terminus, it has a nuclear localization signal (NLS) along with a Huntington, Elongation Factor 3, PR65/A, TOR (HEAT) and Focal Adhesion Targeting (FAT) domain. The ATM gene was first described by Savitsky, et al. (26). The gene is located on chromosome 11q22.3-q23.1 (32). Mutations in the ATM gene causes a rare autosomal disorder called ataxia-telangiectasia (A-T), which is characterized by immunodeficiency, predisposition to cancer, cerebellar degeneration and genome instability (13). In inactivated state, ATM is present as a dimer. With the onset of DNA damage, the inactivated ATM dimer undergoes a conformational change and self

phosphorylates to form a monomer. After self phosphorylation, ATM phosphorylates a number of downstream substrates which in turn induce cell cycle arrest (Figure 2).

Some of the downstream effectors of ATM are c-Abl tyrosine kinase, tumor suppressor gene p53, breast cancer susceptibility gene product BRCA1, the human checkpoint kinase hCds1/chk2, and the Nijmegen Breakage Syndrome gene product NBS1 (18). ATM homologs have also been discovered in *S. cerevisiae*, *S. pombe* and *Drosophila*. They are known as Tel1, Mec1 and Mei1 respectively and play an important role in cell cycle control and response to DNA damage (17). A study in yeast has shown that strains deficient in ATM homolog Tel1p have short telomeres. Only in the presence of Tel1p can short telomeres be elongated (2). Unlike yeast, ATM in mice does not play a very important role in the elongation of short telomeres (6). However, recent studies on telomeres in mice showed that ATM plays an important role in the recognition and processing of dysfunctional telomeres that were created due to the loss of TRF2 (1, 3).

Another protein belonging to the PI3KK family that plays an important role in DNA damage response is Ataxia-Telangiectasia-and-Rad3-related (ATR). Some downstream effectors of ATR protein are p53 and Chk1, which play a role in cell cycle arrest (Figure 2). The ATM and ATR signaling pathways are considered to be very much interlinked. However de Lange and Denchi found that when TRF2 is deleted in cells that lacked ATM kinase activity there was no DNA damage response mediated by ATR (3). They also found that the ATR-mediated pathway was activated when there was a deletion of POT1. However this response was not seen when only ATR levels were reduced. Thus this study established that there were two independent pathways controlling the DNA

5

damage response at telomeres and that the two telomere binding proteins TRF2 and

POT1 played an important role in regulating these pathways (Figure 2).
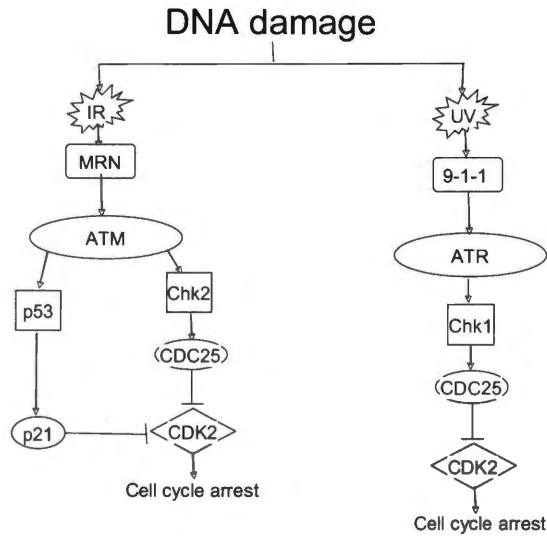
Figure 2. ATM and ATR mediated DNA damage response pathway. The PI3K-like proteins ATM and ATR get activated after induction of DNA damage. ATM phosphorylates Chk2 which inhibits the action of CDC25, leading to the inactivation of CDK2 that subsequently leads to cell cycle arrest. In the ATR pathway Chk1 is phosphorylated by ATR that inhibits the activation of CDC25, subsequently leading to cell cycle arrest because of inactivation of CDK2.

G-Overhang in Telomere Structure

T-loop is formed by inserting single stranded (ss) G-overhang to double stranded (ds) telomeric repeat. The discovery of G-overhang in yeast, humans and mice showed that they are evolutionarily conserved in eukaryotes. The exact significance of the presence of overhangs was not known previously. About a decade ago it was shown that dominant negative mutations in TRF2 lead to reduction of G-overhangs, chromosome fusions and ultimately incur a DNA damage response. Now it is known that the G-overhang is important for the formation of t-loop, along with telomere binding proteins. The G-overhang also serves as a site where telomerase binds and extends short telomeres. However, the process of overhang generation is not fully understood and hence the study of overhang generation is important.

There are several ways by which the generation of G- overhang can be explained. Earlier it was thought that the overhang is present only on the lagging strand due to the end replication problem of linear chromosomes. As described earlier, the end replication problem arises due to the inability of the DNA polymerase to fully synthesize DNA on the lagging strand. Theoretically, at the end of replication the leading strand should be blunt ended and the lagging strand should have a small overhang about the size of RNA primer at the 3′ end. However, it is now known that the overhangs are present on the lagging as well as the leading strand and the length of overhangs is much longer than the length of an RNA primer (19).

One mechanism for the generation of overhang could be attributed to the action of telomerase. However, studies in yeast showed that 3′ overhang was present even in the

absence of telomerase (23, 25). Similarly, knockout mice lacking telomerase activity showed the presence of overhang, leading to the conclusion that the G-overhang can be generated without the action of telomerase (21). Similarly, in human cells not expressing telomerase, G-overhang exists at both telomere ends (7).

Another mechanism for the generation of overhang could be because of the degradation of the C-strand by a nuclease, termed telomere end processing. Evidence has suggested that, in budding yeast, loss of single stranded binding protein POT1 homolog Cdc13p resulted in degradation of C-strand in the $5' \rightarrow 3'$ direction by a nuclease (24). However the nuclease responsible for the degradation of C-strand has not yet been identified. It is also unknown if the same nuclease acts on the leading as well as the lagging strand to generate the overhangs at the two daughter telomeres.

Role of ATM in Telomere End Processing and the Mechanism of G-Overhang
Generation

Verdun et al. (8) have suggested that, at the end of replication, telomere ends are exposed as DNA damage sites to the DNA damage response proteins like MRN, ATM and ATR (Figure 3). The presence of these proteins was further confirmed by partial loss of POT1 from the telomere single stranded region at the G2 phase of cell cycle. It was also shown that inhibition or deficiency of these proteins led to dysfunctional telomeres, thus indicating their roles at the telomeres. Finally, the activation of these proteins did not lead to a normal DNA damage response at the telomeres in the form of non-homologous

end joining (NHEJ), suggesting a possible role in the generation of overhang rather than in inducing a DNA damage response.

Recent evidence has suggested the role of MRN complex in telomere maintenance and in the generation of overhang. Reduced expression of the MRN complex by RNAi leads to transient shortening of G-overhang in telomerase positive cells (7). Since ATM is involved in the same pathway as the MRN complex, it is possible that, like the MRN complex, ATM plays a role in the generation of 3' G-overhang of telomeres. Hence, we postulate that ATM inhibition has an effect on the telomere overhang length and is one of the proteins controlling the telomere overhang length.

In *Saccharomyces*, the generation of single-stranded overhang has been observed in the late S phase of the cell cycle (25). Dionne and Wellinger found that in yeast, the generation of single-stranded overhang is independent of telomerase activity (23). However, in humans, it is not known whether the generation of overhang takes place in the S phase or the G2 phase of the cell cycle and whether this activity is independent of telomerase. The study of cell cycle regulated overhang generation will help us in finding out the cell cycle stage in which the generation of the overhang takes place. Also, studying the cell cycle analysis of overhangs in HeLa and IMR90 cells will enable us to understand the differences if any between the generation of overhang in case of telomerase positive and telomerase negative cells.

Conventional DNA replication generates a blunt end at the leading strand and a short overhang at the lagging. The model suggests that the telomere ends are recognized as a damage site, followed by 5' C strand resection, elongation of G tail and formation of short ss 3' G tail on leading strand.
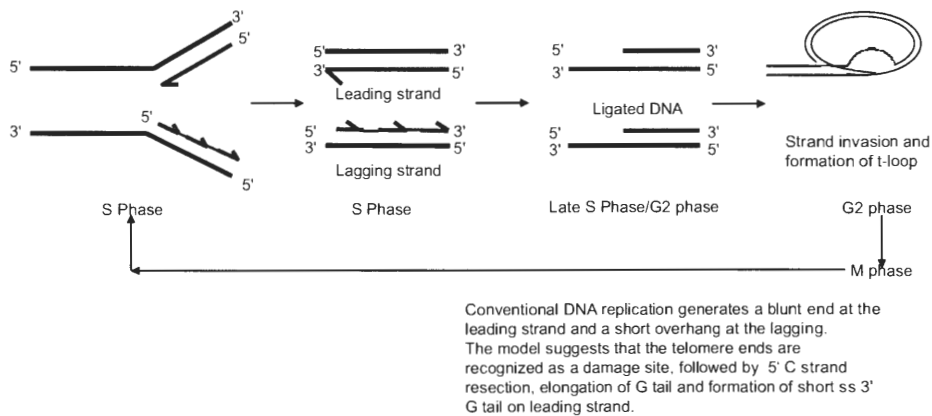
Figure 3. Possible mechanism of G-overhang generation during cell cycle (adapted from, 8). During the S phase DNA replication begins. The leading strand is synthesized continuously in the 5'→3' direction. However there is a problem with the synthesis of the lagging strand. The lagging strand runs in the opposite direction of the leading strand i.e. in the 3'→5' direction and the DNA polymerases are unidirectional, i.e., they can synthesize the complementary strand only in the 5'→3' direction. Hence the lagging strand is synthesized in a discontinuous manner by RNA primer synthesis followed by the formation of Okazaki fragments. RNA primers are then removed and the gaps are filled in by the DNA polymerase. The Okazaki fragments are ligated together by DNA ligase. The end result of DNA replication is the formation of leading strand with blunt ends and lagging strand with a 3' overhang. According to the proposed model, after DNA replication, during the early G2 phase of the cell cycle the telomere ends are accessible to the DNA damage machinery proteins like MRN, ATM, ATR. The chromosome ends are recognized as damaged sites by the damage response proteins and they initiate end resection, generating 3' overhangs. The complete mechanism of overhang generation is unknown but once they are generated they undergo a process that is similar to homologous recombination to generate the t-loop at the G2 phase of the cell cycle.

10

CHAPTER II

MATERIALS AND METHODS

Cell Culture

HeLa human cervical carcinoma cells, BJ human skin fibroblast and IMR90 human fetal lung fibroblast cells were cultured in a 4:1 mixture of Dulbecco's modified Eagle's medium and medium 199 along with 10% cosmic calf serum (HyClone), 0.1% antibiotics (Sigma) and glutamax (Invitrogen) at 37°C in the presence of 5% CO_2.

Cell Synchronization

HeLa cells were synchronized using thymidine and aphidicolin. Cells were grown to 50% confluence in 10 cm dishes. Thymidine (2 mM, stock 100 mM, Sigma) was added. After 16-18 h, thymidine was removed and cells were washed twice with solution A (HEPES, glucose, NaCl, KCl, Na_2HPO_4, pH 7.5). Cells were split in a ratio of 1:3 and were allowed to grow for about 12 h and then aphidicolin (1μg/ml, Sigma) was added. After 12 h, cells were washed three times with solution A and fresh medium was added. Cells were counted and collected at 1.5 h intervals.

IMR90 cells were synchronized using serum starvation-aphidicolin block. Briefly, after the cells reached 50-60% confluence in 15 cm plate, they were serum starved for 48 h. After serum starvation they were released in media containing 20% of cosmic serum and aphidicolin (1μg/ml) for 24h. Cells were then washed with warm solution A twice

11

and released from the aphidicolin block into fresh media containing 20% cosmic serum at 37°C. Cells were collected at regular intervals of 3 h by trypsinization (0.05% trypsin).

After collection of cells, approximately 1 million cells were fixed for fluorescence activated cell sorting (FACS) analysis with 4 ml 70% ethanol. The fixed cells were stored at 4°C until they were used for FACS analysis. For FACS analysis the samples were prepared by first washing with cold PBS and then stained with propidium iodide (Becton, Dickinson and Company) at 37°C for 30 min. FACS analysis was done using DNA acquisition file from the Cell Quest Pro software.

Immunofluorescence

HeLa and BJ cells were plated on a chamber slide (8 chambered slides from LabTekII). Cells were treated with 3 μM or 10 μM of ATM specific inhibitor KU55933 (stock 10 mM) with bleomycin (Roche, 0.2 μg/ml) at 37°C for 1h. After treatment, cells were washed with PBS for a brief period of time and fixed with freshly prepared 4% paraformaldehyde (Sigma) in PBS for 15 min at room temperature. After fixation, cells were washed with PBS 3 times for 5 min each at room temperature. This was followed by permeabilization of cells with 0.1% Triton-X100 (Sigma) in PBS for 10 min at room temperature on a rocker. Cells were again washed with PBS for 5 min each at room temperature (R.T.) on a rocker. The fixed and permeabilized cells were then blocked with 10% BSA (Sigma) in PBS for 1h at 37°C in a humidifying chamber. Subsequently cells were washed with PBS. Cells were then incubated with primary antibody against phosphorylated histone H2AX (γ-H2AX) (prepared in PBS, dilution 1:200, rabbit

12

polyclonal antibody, Calbiochem) for 1 h at 37°C in a humidifying chamber followed by washing 3 times with PBS. Tetramethyl Rhodamine Iso-Thiocynate (TRITC) coupled secondary antibody (prepared in PBS, dilution 1:200, sheep anti-rabbit IgG, Rockland) was then added and incubated at room temperature for 1h. The slide was then washed with PBS 3 times; air dried and mounted using 5µl per slide of Vectashield (Vector Laboratories) containing 4',6-diamidino-phenylindole (DAPI). Prepared slides were observed under Zeiss Axiovert 200M inverted microscope (Carl Zeiss, Inc.) and images were taken using Axiovision-4 software using 100X oil immersion objective.

Quantitation

The number of nuclei containing γ-H2AX positive foci were counted in case of BJ and HeLa cells treated with bleomycin, bleomycin and KU55933 (3 µM and 10 µM) along with control that were treated with DMSO only. Nuclei were considered γ-H2AX foci positive only if the nuclei had 5 or more foci. One hundred nuclei per sample were counted by selecting different fields on the slide. A definite pattern was followed while counting the nuclei to ensure that there was no overlay in the fields. The fields were selected starting from top right hand corner of the slide to the bottom right hand corner in a continuous manner.

Overhang Protection Assay

Genomic DNA for the overhang protection assay was prepared using Qiagen Genomic DNA preparation kit by following the manufacturer's protocol. Before proceeding with the assay the DNA concentration was measured using

spectrophotometer. After measuring the DNA concentration at A_{260} the overhang assay was performed on the samples. For every assay 5 µg of total DNA was suspended in 1X gp32 protection buffer (10 mM HEPES at pH 7.5, 100 µM LiCl, 25mM $MgCl_2$, 50mM $CaCl_2$) and treated with RNase A (Roche, 1µg) with or without ExonucleaseI 3'→5' (NEB, 0.3 U/µg) in 10X gp32 buffer supplemented with β mercaptoethanol (and incubated at 37°C for 1 h to overnight) to remove the 3' overhang from the total DNA.

Single-stranded DNA was coated with T4 gene protein 32 (Roche, 10 pmol/µl) for one hour at room temperature. Glutaraldehyde (0.025%) was used for crosslinking at room temperature for 15 min. Crosslinking was stopped by adding 0.45 µl 1 M Tris (pH 7.5). The double stranded unprotected DNA was digested by adding DNAse I (Roche, 0.0025 U/µl) for 30 min at 37°C followed by inactivation of DNAseI at 80°C for 30 min. After the completion of DNAseI treatment, samples were treated with Protease K (NEB, 1 µg/µl) and Sodium Dodecyl Sulfate (SDS, 0.5%) at 55°C overnight for the digestion of proteins and reverse crosslinking. High-specificity C-rich probe was prepared and added to the samples. The samples were left overnight at room temperature for hybridization. The C rich probe was prepared by annealing G rich template oligo containing uracil (1.7 pmol/µl), with oligonucleotides (dAdT, 1.25mM), which was extended by Klenow (large fragment of DNA polymerase 5U/µl) in the presence of α-^{32}P-dCTP (3000Ci/mmol). This reaction mixture was allowed to stand at room temperature for 15 min followed by heating at 95°C for 5 min in a heating block for the inactivation of Klenow. Finally, for obtaining the probe, 0.5 µl of uracil deglycosylase (UDG) (NEB, 1U/µl)) was added to remove the G rich template. After UDG treatment, the probe was tested on a 20%

14

polyacrylamide gel. For assay, the probe was diluted by adding the original probe to 10X gp32 buffer and water.

After overnight hybridization with the probe, samples were analyzed on a 6% polyacrylamide gel (premade and stored at 4°C) at 4°C in 0.5X Tris-Borate-EDTA (TBE) buffer for 2.5 h at 300V. The gel was dried on a hybond N+ membrane (Amersham Biosciences Limited) at 55°C for approximately 2 h on a gel drying slab. The dried gel-membrane assembly was exposed to PhosphorImager screen (Kodak). The screen was scanned the next day, using molecular FX imager (Bio-Rad). The scanned document was quantitated using ImageQuant software (GE Healthcare). Size standards, both treated (protected) and untreated were included in the experiment to confirm consistent protection.

Quantitation of Overhang Protection Assay

The quantitation of the scanned image was done by opening the image in Imagequant software. A grid of 30 boxes was overlaid on the scanned gel picture (Figure. 4). Signal intensity for each box was obtained with this software. The signal intensity values were then transferred to the program that calculated the weighted mean size of the overhang. The formula that was used in the program was $\sum(OD_i)/\sum(OD_i/L_i)$ where OD_i refers to the signal intensity and L_i refers to the length of DNA in nucleotides at that position using the size of the molecular weight markers at different positions as a standard (7). The program can be accessed at the following website: (http://www.swmed.edu/home_pages/cellbio/shay-wright/research/1UTSWTelorunforweb.xls)

15
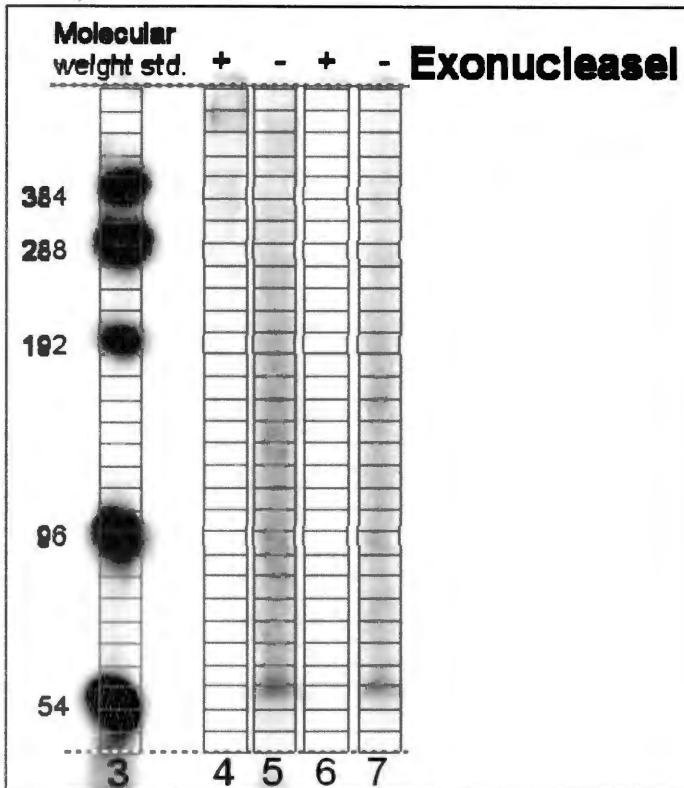
Figure 4. Sample quantitation of telomere overhang protection assay. The gel is first overlaid with a grid of boxes and quantitated using ImageQuant software. To measure the size of the overhang the ExoI treated samples are used as background and their signal is subtracted from that of the untreated sample at each measured size interval. The weighted mean size is calculated by using the formula $\sum(OD_i)/\sum(OD_i/L_i)$ where OD_i refers to the signal intensity and L_i is the length in nucleotides of the DNA at that position i using the range of molecular weight standards.

In-Gel Hybridization

After treating the genomic DNA with or without *E. coli* Exonuclease I (NEB, (10U/μl) at 37°C for 60 min to overnight, the samples were incubated with Protease K (NEB, 20mg/ml) and 10% SDS at 55°C overnight. The next day, samples were hybridized to a C- rich probe overnight. The samples were separated on a 0.7% agarose

gel at 4°C followed by denaturation of the gel by washing with 0.5M NaOH and 1.5M NaCl for 45 min at 4°C. The gel was rinsed with water for 10 min at 4°C. Further, the gel was dried on a hybond N+ membrane (Amersham Biosciences) at 55°C for about 1.5 h on a gel drying slab. After drying the gel on the membrane, the membrane was exposed to PhosphorImager screen (Kodak) overnight. The gel was put in a neutralization buffer for 15-30 min at room temperature. The hybridization chamber was set to 42°C. After the neutralization step, the gel was transferred to the hybridization chamber in a bottle along with the Alu probe overnight. Alu probe was prepared by adding Alu (oligo) 10µM, 10X kinase buffer, γ-^{32}P ATP, water and T4 kinase (10,000 U/ml) to a microfuge tube and the mixture (probe) was kept at 37°C in a heating block for 30 min. The probe was finally added to desired amount of hybridization buffer and was ready to use.

After overnight hybridization with Alu probe, next day the gel was washed with 0.1X SSC and 0.1% SDS, 2 times for 15 min at 25°C in the hybridization oven. The gel was exposed to phosphor screen imager for an hour. The imager screens were scanned using Molecular FX scanner (Bio-Rad) and the scanned images were quantitated using Quantity One software program. The overhang abundance was calculated by normalizing the signals from the membrane with the Alu repeat signal from the gel.

In both in-gel hybridization and overhang protection assay, the Exonuclease I treated samples served as background and its signals were subtracted from that of the untreated sample.

CHAPTER III

RESULTS

ATM Signaling Pathway Does Not Play a Role in the Maintenance of Telomere

Overhang

To determine the role of ATM in telomere overhang maintenance in humans, an ATM kinase specific inhibitor KU55933 was used (11) to inhibit ATM kinase activity. The effect of this inhibition was seen by performing immunofluorescence for the presence of γ-H2AX. H2AX is one of the downstream effectors of ATM. Phosphorylation of H2AX is one of the first steps in the DNA damage response pathway that requires the ATM kinase activity. γ-H2AX marks the DNA damage site and subsequently recruits a number of target proteins like 53BP1, BRCA1, Nbs1 at the damaged site, forming a large protein complex that can be detected under microscope.

Cells were first exposed to DNA double strand break inducing agent bleomycin and then were treated with different concentrations of the ATM kinase inhibitor KU55933 (3 and 10 μM). Bleomycin treatment generates DSB that induces the phosphorylation of H2AX via ATM at the damage site. This leads to formation of γ-H2AX foci at the DSB. Immunoflourescence results showed that when cells were treated with bleomycin, γ-H2AX foci took place due to the induction of DNA damage. Foci formation was not observed in case of cells that were treated with DMSO only. The foci

formation was partially inhibited with 3μM of KU55933 and was completely inhibited at a higher concentration of 10μM, suggesting that the ATM kinase activity was inhibited by KU55933. Figure 5 top panels represent HeLa cells treated with bleomycin (0.2 μg/ml) that show γ-H2AX foci formation in addition to HeLa cells treated with DMSO as a control. Figure 5 bottom panels show cells treated with bleomycin that show the absence of γ-H2AX foci formation as a result of ATM kinase inhibitor treatment with KU55933 at 3 and 10 μM concentration. In Figure 6 top panels show γ-H2AX foci formation in BJ cells treated with bleomycin along with the DMSO treated cells as a control. Figure 6 bottom panels show BJ cells treated with ATM kinase inhibitor KU55933 at 3 and 10 μM concentration in addition to bleomycin that do not show any γ-H2AX foci formation. A total of 100 nuclei were counted in case of each treatment group and a graph was plotted using the treatment given to cells against the percentage of foci positive nuclei counted in each sample (Figure 7).
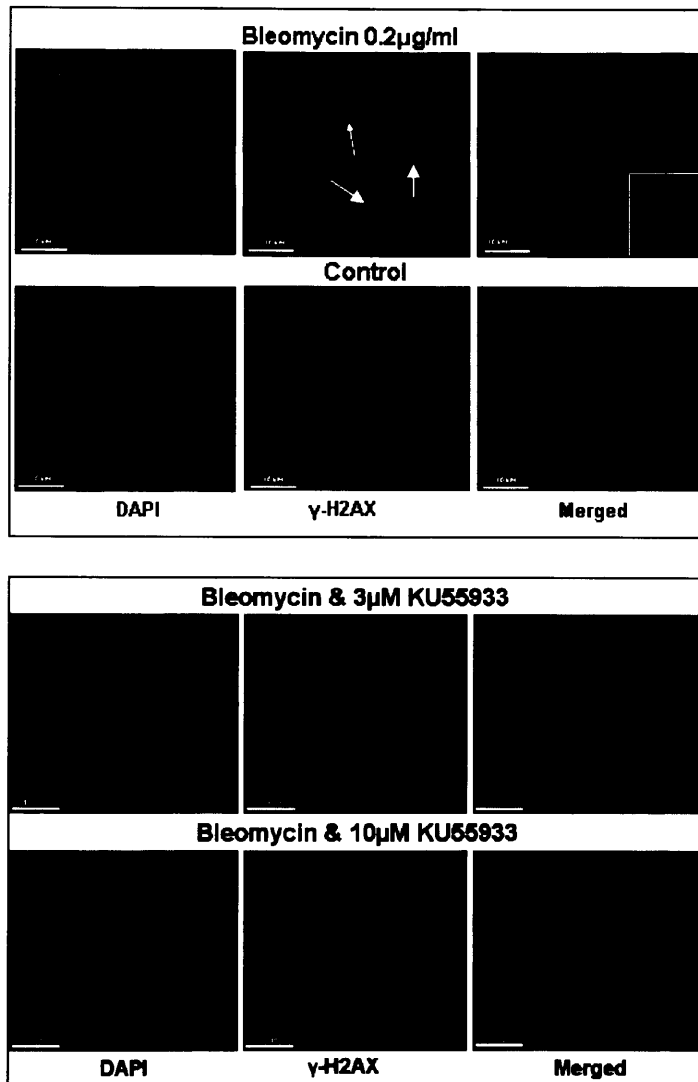
Figure 5. HeLa Immunofluorescence. Top panels show γ-H2AX foci formation (arrows in white) in HeLa cells that were treated with bleomycin (0.2 μg/ml) and control cells that were treated with DMSO only, which were devoid of any foci. Bottom panels show HeLa cells treated with different concentrations of KU55933 along with bleomycin. The KU55933 concentrations used were 3 and 10 μM. No foci formation was observed in cells that were treated with 10 μM but a few foci were observed in case of cells that were treated with 3 μM of KU55933, indicating that at 10 μM KU55933 concentration ATM kinase activity was completely inhibited. The inset shows a nucleus with γ-H2AX foci formation in bleomycin treated cells. Scale bar: 10μm.

20
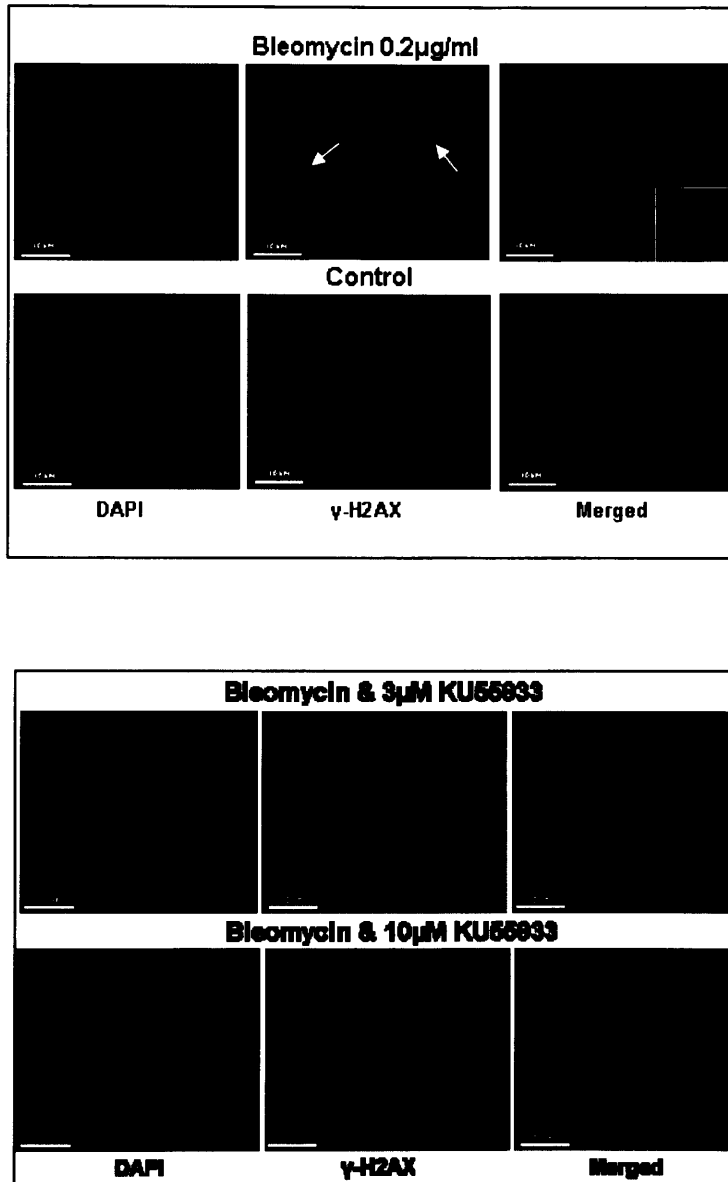
Figure 6. BJ Immunofluorescence Top panels show human foreskin fibroblast BJ cells treated with bleomycin that showed the formation of γ- H2AX foci (arrows in white). Also, BJ cells treated with DMSO as a control with no foci formation are seen. Bottom panels show BJ cells treated with 3 μM and 10 μM of KU55933. No foci formation was observed in case of BJ cells treated with 10 μM of KU55933 but at 3 μM KU55933 a few foci were observed. The inset shows a nucleus with γ-H2AX foci formation in bleomycin treated cells. Scale bar: 10μm.

21
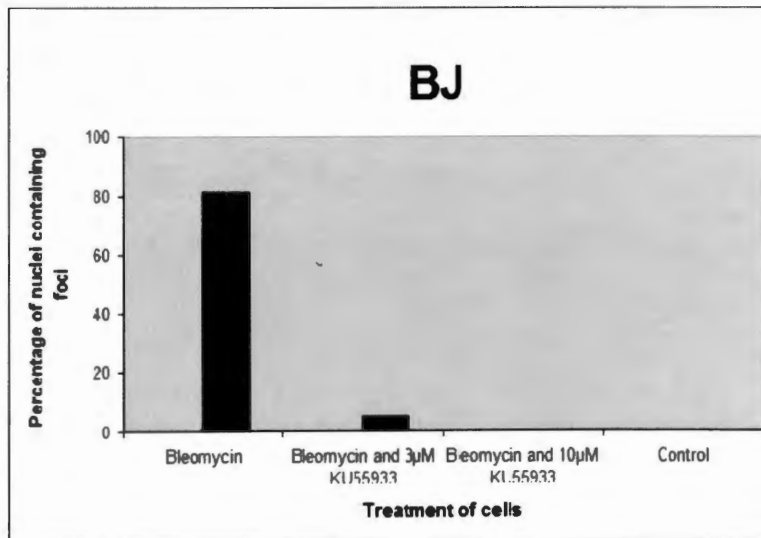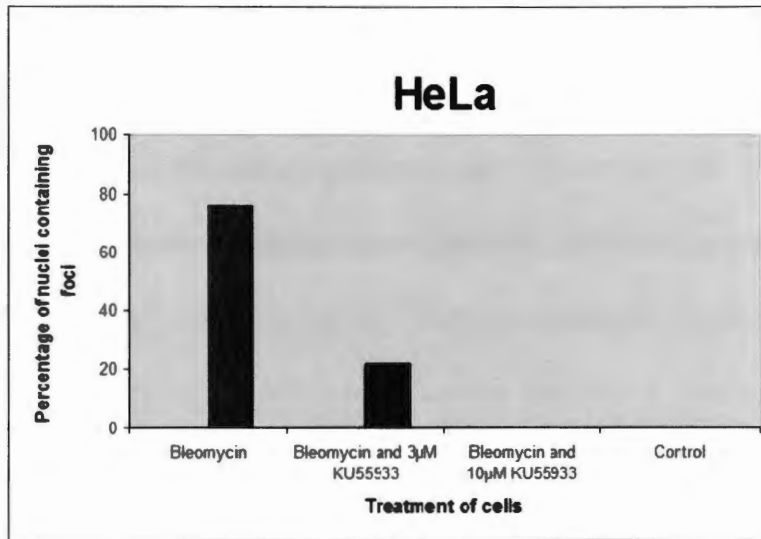
Figure 7. Graph representing Immunoflourescence results in HeLa and BJ cells. KU55933 10 µM inhibits the action of ATM in HeLa (top) and BJ (bottom) cells. HeLa and BJ cells were seeded on an 8 chambered slide and were treated with the DNA damage inducing agent bleomycin (0.2 µg/ml) along with 3 and 10 µM concentration of ATM inhibitor KU55933. DMSO treated cells served as a negative control for this experiment. The cells were then subjected to immunofluorescence for γ-H2AX. Total 100 nuclei were counted for each sample and the numbers of γ-H2AX foci were compared in all samples. A graph was plotted with the indicated treatments against the percentage of foci positive nuclei.

Telomere overhang protection assay was done using both the concentrations of 3 and

10μM of the ATM inhibitor to observe the effect of ATM kinase inhibition on the mean

overhang length. HeLa and BJ cells were treated 48h with the inhibitor along with

DMSO as a control. Telomere overhang protection assay was then used to measure the

mean overhang size of the telomeres. Figure 8 shows the scanned image of the gel. In the

figure, the telomeric overhang DNA is seen as a smear between a given range of

molecular weight markers. The scanned image was quantitated using ImageQuant

software and the program mentioned in chapter II. After performing two independent

experiments it was noticed that the ATM kinase inhibition did not have a significant

effect on the mean telomere overhang length as represented in the graph in Figure 9.
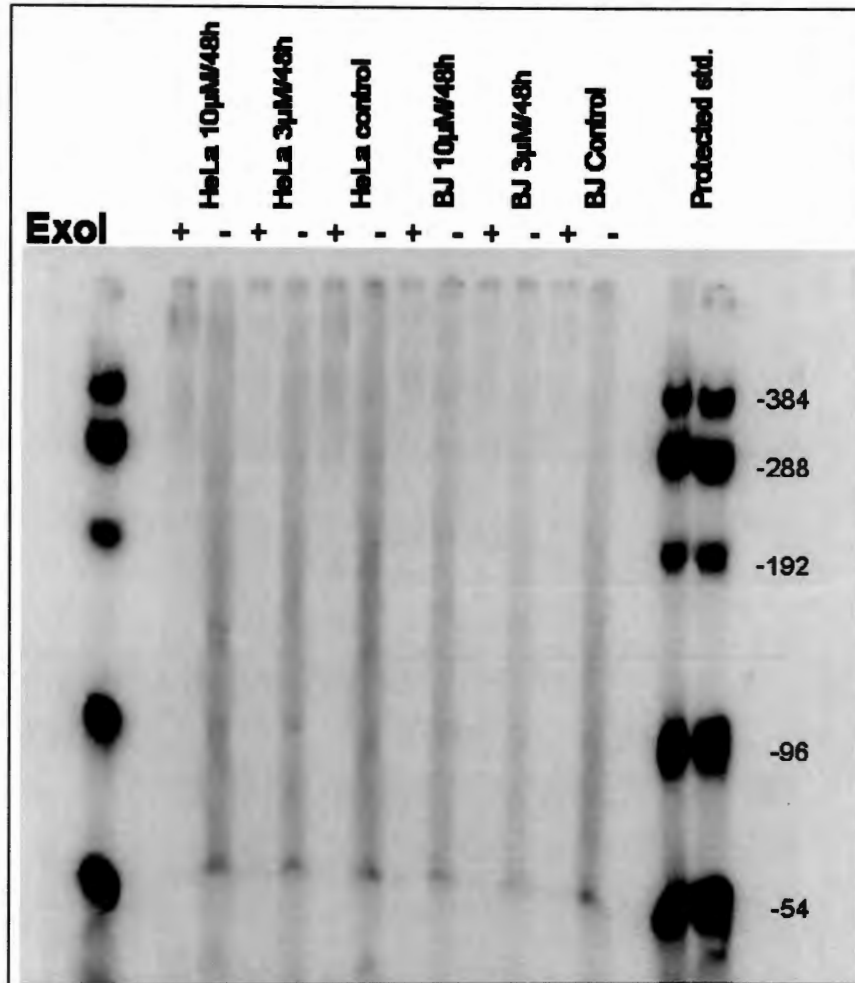
Figure 8. Telomere overhang protection assay on KU55933 treated HeLa and BJ cells. ATM inhibition did not change the telomere overhang length. HeLa and BJ cells were subjected to ATM inhibition by ATM specific inhibitor KU55933. Genomic DNA was prepared from the treated samples. Telomere overhang protection assay was done using the same samples. In the scanned gel picture above, intensity of the smear indicates the bulk of telomere overhang DNA present at that position. In the figure every alternate lane with no signal is the ExoI treated sample (thus, the ExoI untreated samples show the telomere overhang signal in the form of a smear). ExoI removes the single-stranded DNA in $3' \rightarrow 5'$ direction, therefore removing G-overhang. These served as a background while calculating the mean telomere overhang length.
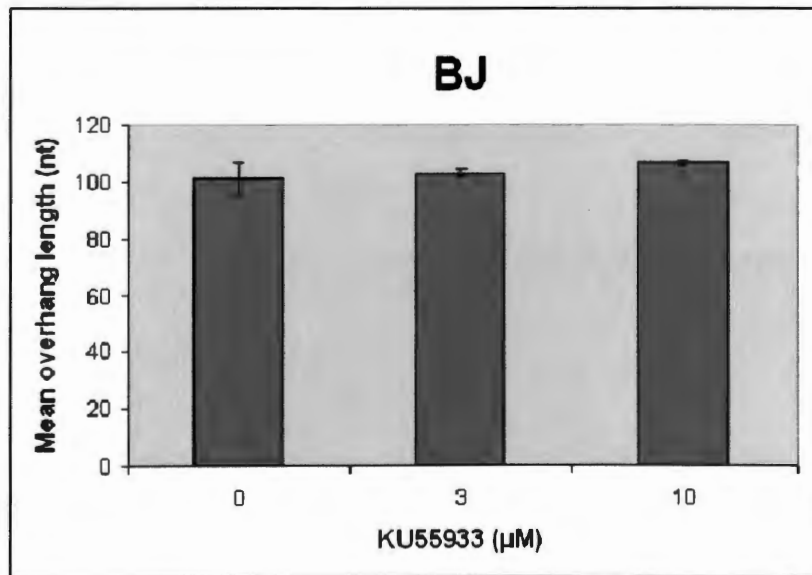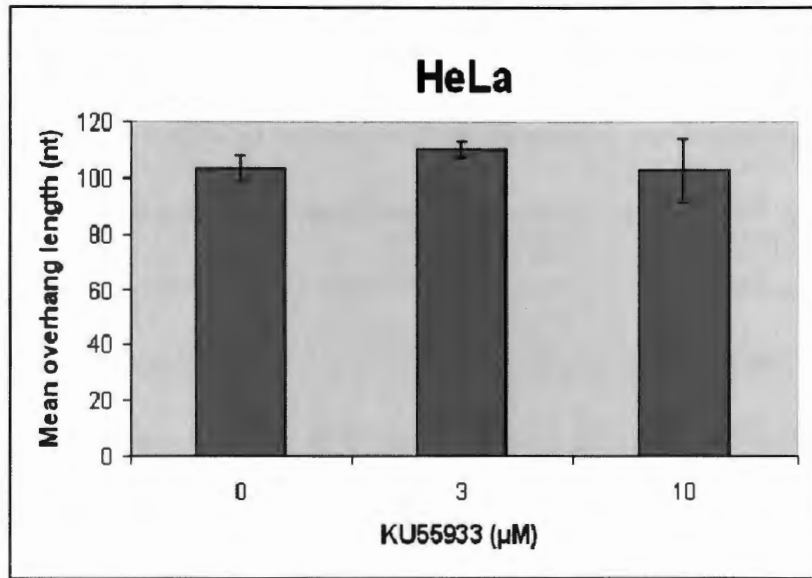
Figure 9. Graph representing the effect of ATM kinase inhibition by KU55933 on HeLa and BJ cells. ATM kinase inhibition has no effect on the telomere overhang length in case of HeLa and BJ cells. HeLa and BJ cells were treated with ATM kinase specific inhibitor KU55933 for a period of 48 h and subsequently genomic DNA extracted, was subjected to telomere overhang protection assay that measures the mean overhang length. The bar graphs above indicates that the mean overhang length in case of HeLa as well as BJ cells treated with 3 and 10μM of Ku55933 did not change in comparison to the control cells. Graphs represent two independent experiments done to calculate the mean overhang length.

In-gel hybridization assay was done to measure the telomere overhang abundance using HeLa DNA subjected to KU55933 inhibition. The experiment was repeated several times. Scanned images of gel (representing total genomic/Alu signal) and membrane (representing membrane signal) along with the graph are shown in Figure 10. The scanned gel and membrane images were quantitated using quantity one software program. However, the data obtained from the assay gave rise to inconsistent results. Hence, measuring the telomere overhang length overhang protection assay was used in the subsequent experiments for the telomere overhang measurement.
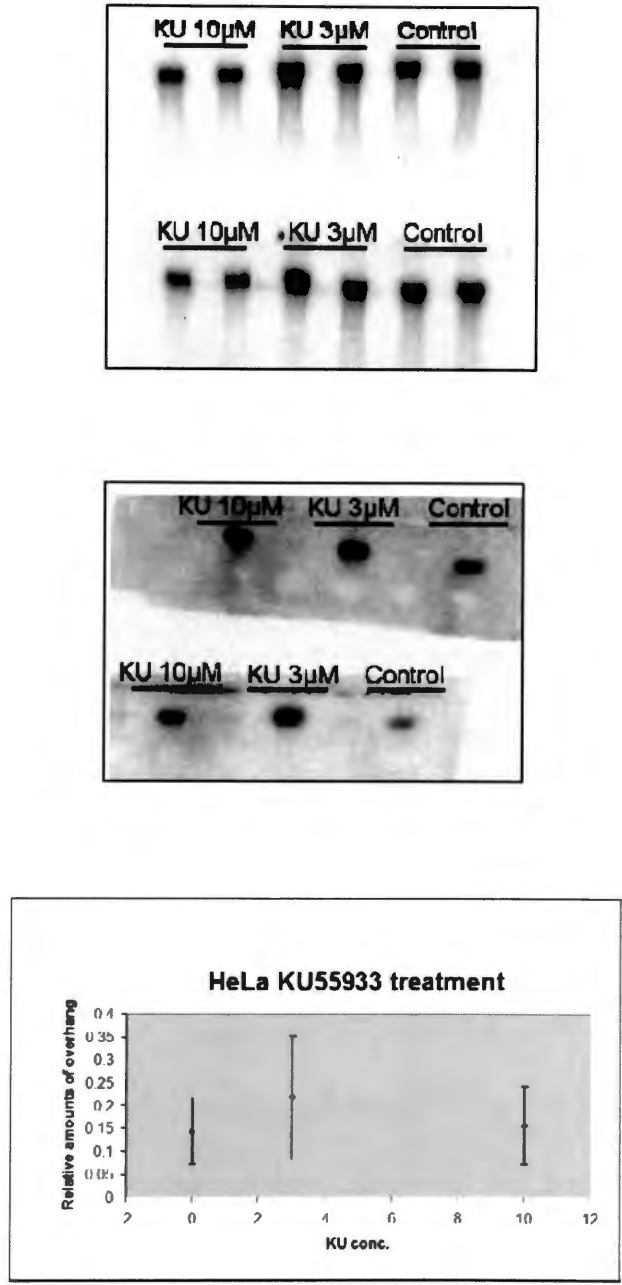
Figure 10. In-gel hybridization assay to measure telomere overhang abundance in KU55933 treated HeLa cells. ATM kinase inhibition does not have any effect on the telomere overhang using the in-gel hybridization assay. First image from top is the scanned image of gel representing the Alu repeat signal. Second scanned image is of the membrane representing the telomere overhang signal. The graph represents relative amount of overhangs that were calculated by normalizing signals from the membrane (overhang signal) to the Alu signal (total genomic DNA). Graph represents more than three independent experiments done to calculate the relative amount of overhang.

The G-Overhang Generation Takes Place in Late S/G2 Phase of the Cell Cycle

For studying the exact phase in which the generation of the 3′G-overhang takes place in human cells, HeLa cells were synchronized using the thymidine-aphidicolin block. Cells were collected after every 1.5h time interval and fixed with 70% ethanol. Fixed cells were stained with propidium iodide and the synchronization was checked by FACS. From the histograms in Figure 11 it can be seen that after 3h of release from the aphidicolin block (early S phase) cells proceeded to mid-S phase of the of the cell cycle. Entry into G2 phase was achieved by the end of 6h and subsequently cells entered the M phase seen by doubling of the DNA content. After extraction of genomic DNA from the synchronized cells, telomere overhang protection assay was carried out. Figure 12 shows the image of a scanned gel showing the distribution of telomere overhang signal. The figure also shows that there was a gradual increase in the mean size of the overhang after the release of cells from mid-S phase (i.e., at 3h time interval). Interestingly the mean size of the overhang peaked at late S and early G2 phase (i.e., at 6h and 7.5h time interval) of the cell cycle and then gradually decreased by the end of G2 phase, indicating that the overhang is most likely being processed during the late S and early G2 phase of the cell cycle (Figure 13).
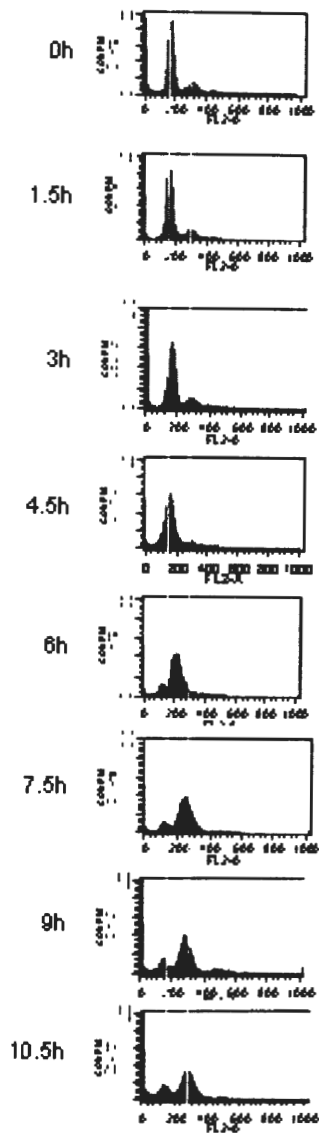
Figure 11. HeLa cell synchronization. HeLa cells were subjected to synchronization at early S phase using thymidine-aphidicolin block. The cells were released from the block and were collected at every 1.5h. The cells were then fixed in 70% ethanol and stored at 4°C. The cells were then stained with propidium iodide for 30 min at 37°C. The synchronization was then checked using the FACSCalibur from Becton- Dickinson. The above histograms show the gradual entry of cells into the subsequent stages of the cell cycle at specific time intervals. At 0h majority of the cells are in the early S phase followed by entry in the G2 phase by the end of 6h. By 10.5h cells are into the M phase of the cell cycle as the DNA content appears to be doubled.

29
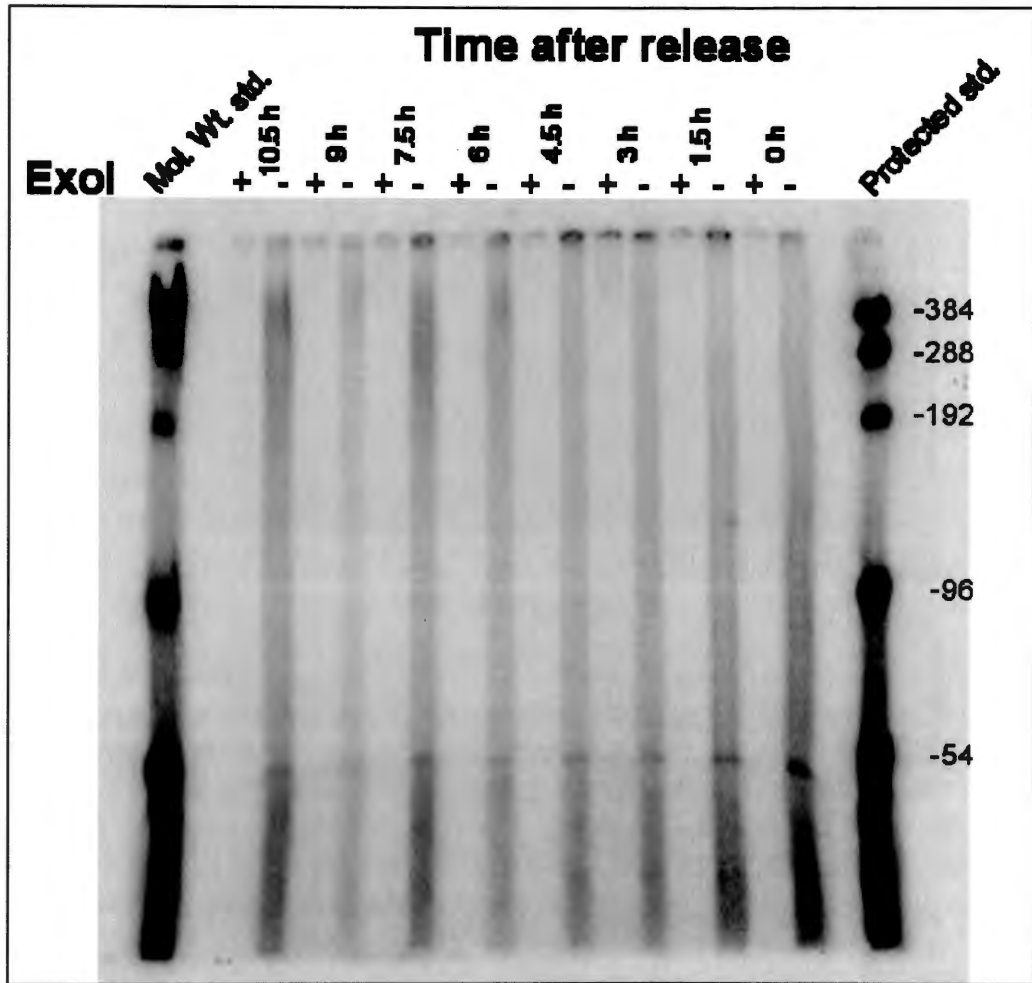
Figure 12. Cell cycle analyses of telomere overhang in HeLa cells. The mean telomere overhang length increases in the late S/G2 phase of the cell cycle. Overhang protection assay using DNA from the synchronized HeLa cells was done to measure the mean telomere overhang size. The extreme right and left hand side lanes are the molecular weight standards used for checking protection. Every alternate lane in the image is the ExoI treated lane that serves as a background while calculating the mean telomere overhang length. The amount of G-overhang at high molecular weight (384-192 bp) increased as cells progressed from early S to late S phase and G2 phase of the cell cycle.

30
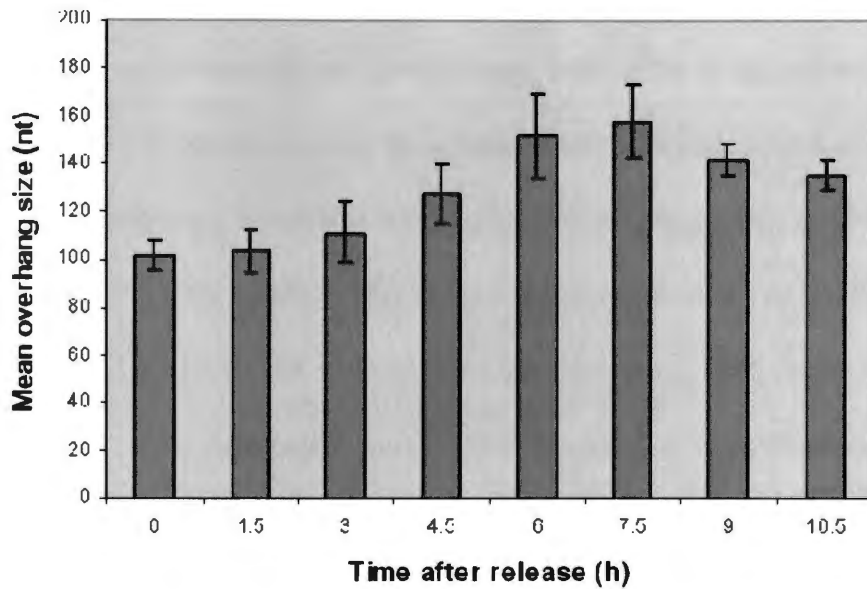
Figure 13. Graph representing cell cycle analyses of telomere overhang in HeLa cells. Telomere overhang protection assay was performed on the synchronized HeLa genomic DNA samples. Time in hours after release from the thymidine-aphidicolin block is plotted against the mean size of the overhang. The mean overhang size in synchronized HeLa cells increased at late S/G2 phase of the cell cycle i.e., the 6h and 7.5h time points. Graph represents two independent experiments.

The Process of G-overhang Generation Is Independent of Telomerase Activity

Studies in yeast showed that the overhangs exist in the strain lacking telomerase activity. Since the process of overhang generation is not fully understood in case of human cells, it is important to analyze whether telomerase plays a role in G-overhang generation. We then tested whether telomerase affect the cell cycle-regulated G-overhang alteration observed in HeLa cells. Telomerase negative somatic cells, human fetal lung fibroblasts IMR90, were subjected to synchronization using serum-starvation followed by aphidicolin treatment to block the cells in early S phase. Aphidicolin was then removed and cells were released to S phase. Figure 14 shows histograms at specific time interval of 3h. Telomere overhang protection assay was performed on the synchronized IMR90 DNA samples (Figure 15). Quantitation showed that the mean overhang length increased by the late S phase and G2 phase and again decreased as the cells proceeded to the subsequent stages of the cell cycle (Figure 16), similar to the cell cycle-regulated G-overhang change in HeLa cells. Thus it could be concluded that the generation of overhangs occurred in the late S and G2 phase of the cell cycle independent of telomerase activity.
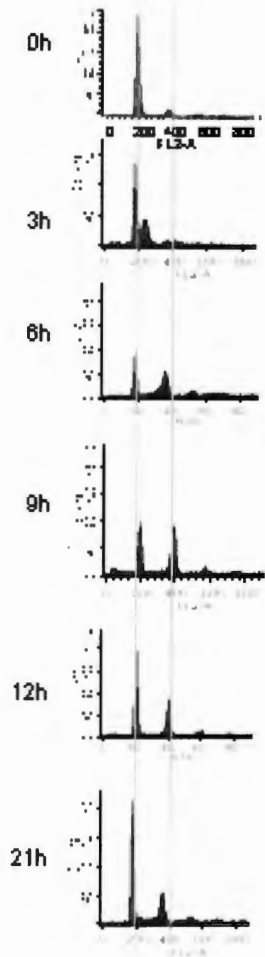
Figure 14. IMR90 cell synchronization. IMR90 cells were subjected to synchronization using serum-starvation and aphidicolin method at early S phase. IMR90 cells were plated on 15 cm plates and after reaching correct confluence were subjected to 48h of serum starvation. After 48h the cells were released into fresh media and were again blocked at early S phase using aphidicolin for 21 h. After 21h the cells were released in fresh media and samples were collected every 3 h up to 21 h for FACS analysis and G-overhang measurement. The cell synchronization was checked by FACS. Histograms show progression of the cell cycle through different phases, starting from 0h at which the cells are at the early S phase to the 21h time interval at which most of the cells are in the M phase of the cell cycle.

33
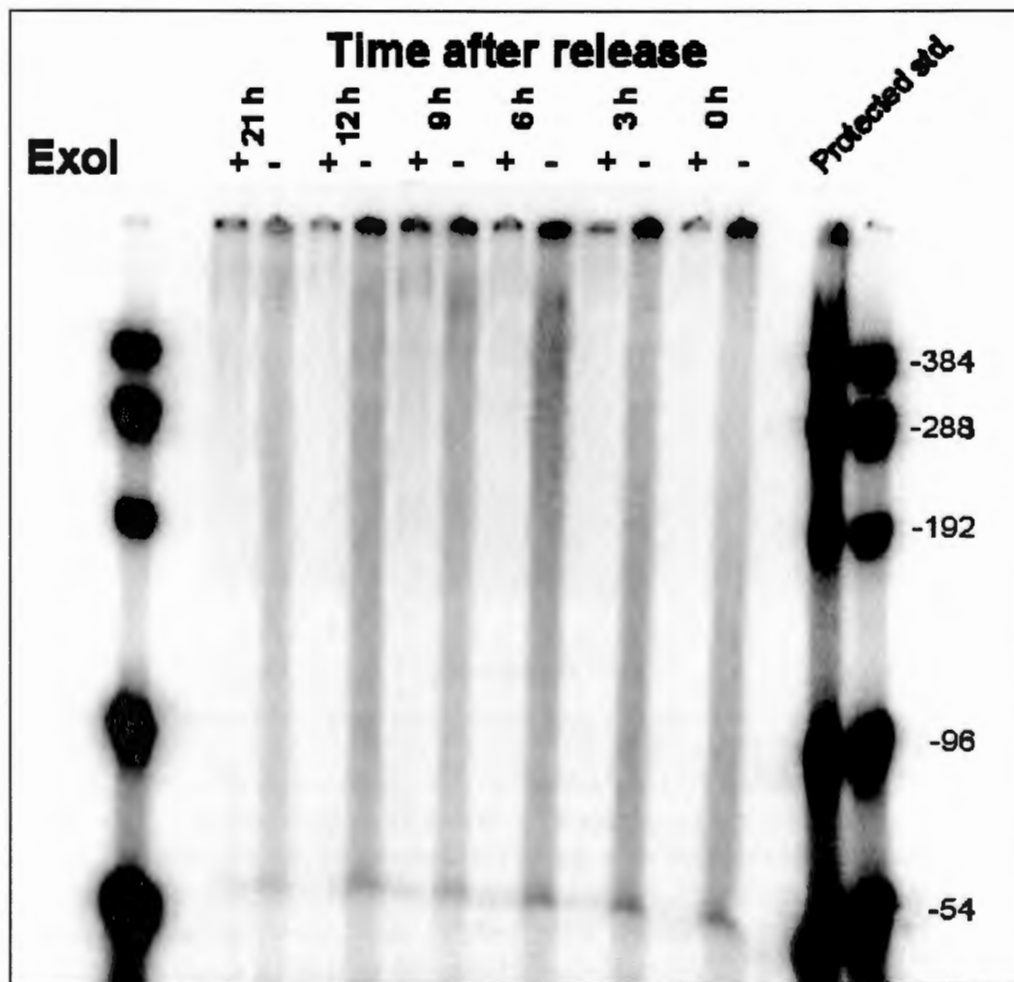
Figure 15. Cell cycle analyses of telomere overhang in IMR90 cells. Telomere overhang protection assay was carried out on the DNA from the synchronized IMR90 cells. Molecular weight markers were used in the experiments and one of them was subjected to overhang protection. Every alternate lane represents the ExoI treated lanes that served as a background while calculating the mean overhang length. The extreme right and left lanes are the molecular weight standards.
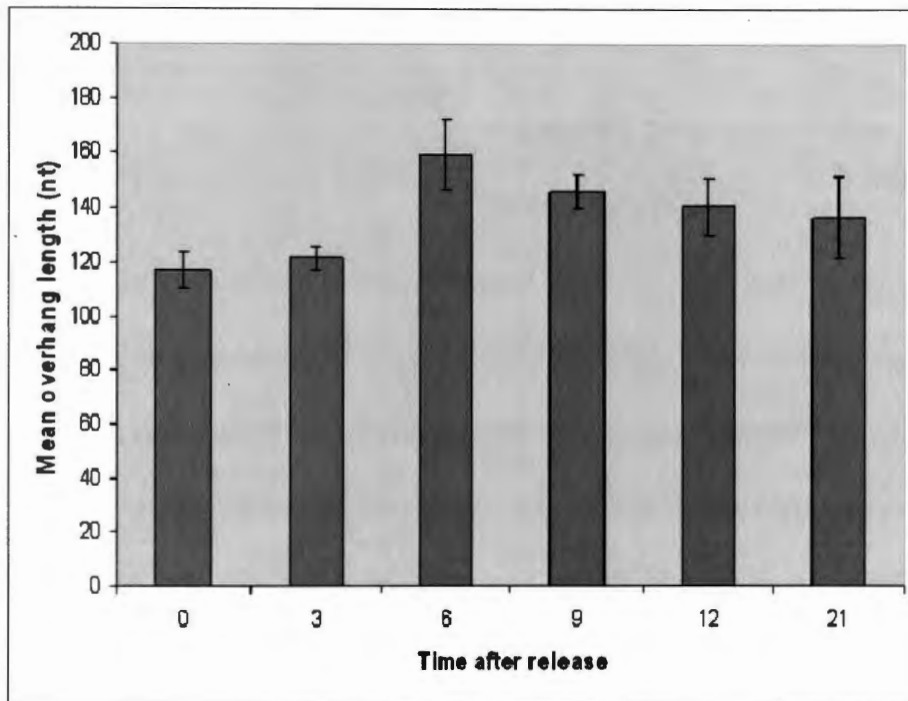
Figure 16. Graph representing cell cycle analyses of telomere overhang in IMR90 cells. Cells were synchronized at G1/early S phase boundary and then released to S and G2 phase. Telomere overhang protection assay was performed on the genomic DNA from synchronized IMR90 cells. The mean telomere overhang length was found to increases at the late S (i.e. at the 6h time interval after release) and G2 phase (i.e. at the 9h time interval) of the cell cycle in the telomerase-negative IMR90 cells. Graph represents two independent experiments. The graph is plotted as time after release from the aphidicolin block against the mean overhang length (nt).

35

CHAPTER IV

DISCUSSION

The G-overhang is known to play an important role in the formation of t-loop and in the telomerase mediated elongation of telomeres. The formation and maintenance of overhang is therefore an important event. The model suggested by Verdun et al. (8) showed that telomere ends are recognized as DNA damage sites during the G2 phase of the cell cycle by DNA damage response proteins like MRN, ATM and ATR. Though these proteins do not bring about a DNA damage response, they are still found at the telomere ends, suggesting a role at the telomere ends. Chai et al. (7) showed that deficiency in the MRN complex led to transient reduction of the G-overhang length. Since ATM and MRN are known to be participants of the same signaling pathway in response to DNA damage, it was speculated that inhibiting the ATM kinase protein would have an effect on the telomere G-overhang length.

In this study, the effect of ATM kinase inhibition on the G-overhang length was determined using the ATM kinase specific inhibitor KU55933 by telomere overhang protection assay that measures the mean overhang length. The effect of ATM kinase inhibition was studied in normal/somatic (BJ) as well as cancer cells (HeLa) at a concentration of 3 and 10 μM KU55933. Results suggest that ATM kinase inhibition have no effect on the telomere overhang length irrespective of the cell type. From my studies it can be concluded that inhibiting ATM kinase activity by the ATM kinase

specific inhibitor KU55933 does not have any effect on the telomere overhang length (Figure 9), suggesting that ATM signaling pathway most likely does not play a role in generating G-overhang length, i.e. ATM signaling pathway may not play a role in telomere end processing.

Though it is generally thought that the ATM and ATR signaling pathway operate separately, it is possible that ATM and ATR might be players of the same signaling pathway also involving Mre11 (of MRN complex). Studies showed that ATM and Mre11 enhance ATR signaling pathway. With the absence of ATM and Mre11 the ATR dependent Chk1 phosphorylation is defective thus indicating a connection between ATR and the Mre11 and ATM signaling pathway (42). These observations give rise to a possibility that instead of the ATM signaling pathway, ATR signaling pathway might play a role in telomere end processing. Another possibility is that the maintenance of telomeres might be interdependent on the ATM and ATR pathways rather than involving just one signaling pathway. Hence inhibiting the action of any one protein does not have any effect on the telomere overhang length. However, it needs to be confirmed that ATR inhibition does not have any effect on telomere overhang length before such a conclusion can be reached.

It was studied that, in yeast, the telomere overhang generation takes place in the late S phase of the cell cycle after the conventional DNA replication. The overhangs were found on both lagging as well as leading strands of the chromosome and the event of G-overhang generation was found to be independent of telomerase activity (25). The mechanism of overhang generation was studied by constructing two linear plasmids with

37

one having the origin of replication and one without the origin of replication. By two-dimensional agarose electrophoresis and Southern blot analysis it was shown that the G-overhang generation was seen only in the plasmid that had the replication origin. Thus, it was inferred that the 5′ C strand resection activity required for the formation of G-overhang was dependent on the passage of replication fork machinery and was thus cell cycle dependent (40).

In ciliates it was shown that the telomere overhang generation is not a telomerase mediated event. Studies carried on the mechanism of overhang generation in *Tetrahymena* showed that the G strand was processed by a cleavage reaction like the C strand resection process for the generation of overhang (14) and that the nuclease responsible for these reactions is not sequence specific.

In humans it is unknown whether the G-overhang generation is cell cycle regulated. I therefore analyzed G-overhang generation in human cells. The cell cycle analysis of overhangs in IMR90 (telomerase negative) and HeLa (telomerase positive) cells showed that elongation of the G-overhang takes place in the late S/G2 phase of the cell cycle. Comparison between the G-overhang generation in cancer cells and normal cells also showed that telomerase expression did not alter the cell-cycle regulated G-overhang elongation, thus indicating that the G-overhang generation is independent of telomerase activity. Thus in humans, the process of G-overhang generation is independent of telomerase activity and is cell cycle stage dependent as in other organisms but the cell cycle stage and the mechanism of G-overhang generation seems to be different in humans.

I think that the generation of overhang in humans can be attributed to two mechanisms. One mechanism could be that the replication fork collapses before it reaches the end of telomere. This could lead to the formation of longer G-overhangs on lagging daughter telomeres in S phase, which can then be filled in by the DNA polymerases in the subsequent cell cycle stage, giving rise to a comparatively shorter 3' overhang (Figure 17). However, on the leading daughter strand, collapse of the replication fork would generate a 5' C-rich overhang. The 3' G-overhang at the leading daughter telomeres could then be generated by extensive C-strand resection by an unknown nuclease (Figure 17).

Alternatively, replication machinery can synthesize telomere DNA all the way to the ends. Then, extensive nuclease digestion on the leading and lagging strands in the late S/ G2 phase of the cell cycle can give rise to longer overhangs. After G2 phase, a fill-in synthesis at C-rich strand, probably by the conventional DNA replication machinery proteins generate shorter G-overhangs (Figure 18). Further, since the intermediate products of the two mechanisms of overhang generation suggested are different, different assays can be employed to study to find out the actual mechanism operating at the telomere ends leading to the generation of the overhang.

My study contributed in understanding the process of telomere end processing and DNA damage pathway. Such studies will ultimately help in finding out solutions to curb shortening of telomeres and thus help in avoiding premature senescence. On the other hand it will also help in finding out various ways of promoting telomere shortening in cancer cells.
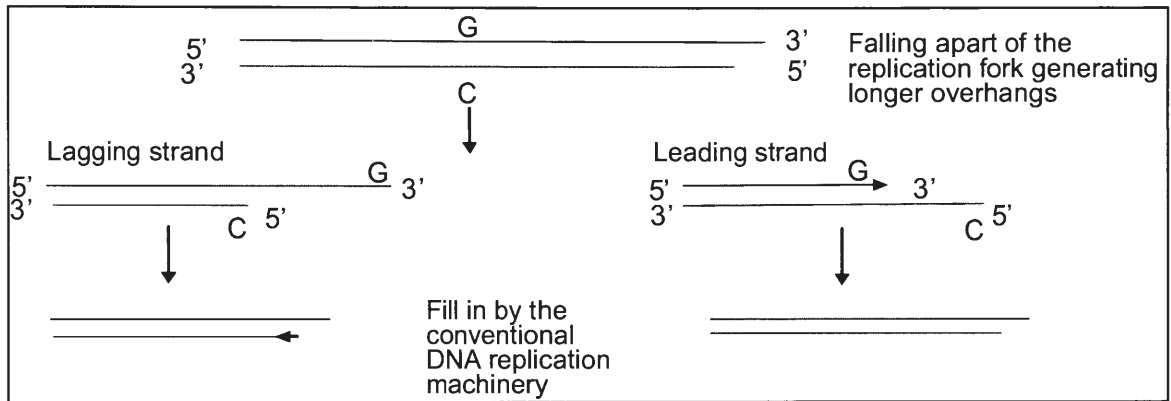
Figure 17. Proposed mechanism of G-overhang generation in human cells. Long overhangs on the leading and lagging strands could be generated due to the collapse of the replication fork machinery during the late S phase of the cell cycle. In the later phase of the cycle on the lagging strand, fill-in synthesis by the DNA replication machinery could give rise to a short 3′ overhang. Possibly C strand resection on the leading strand could be responsible for overhang generation on the leading strand.
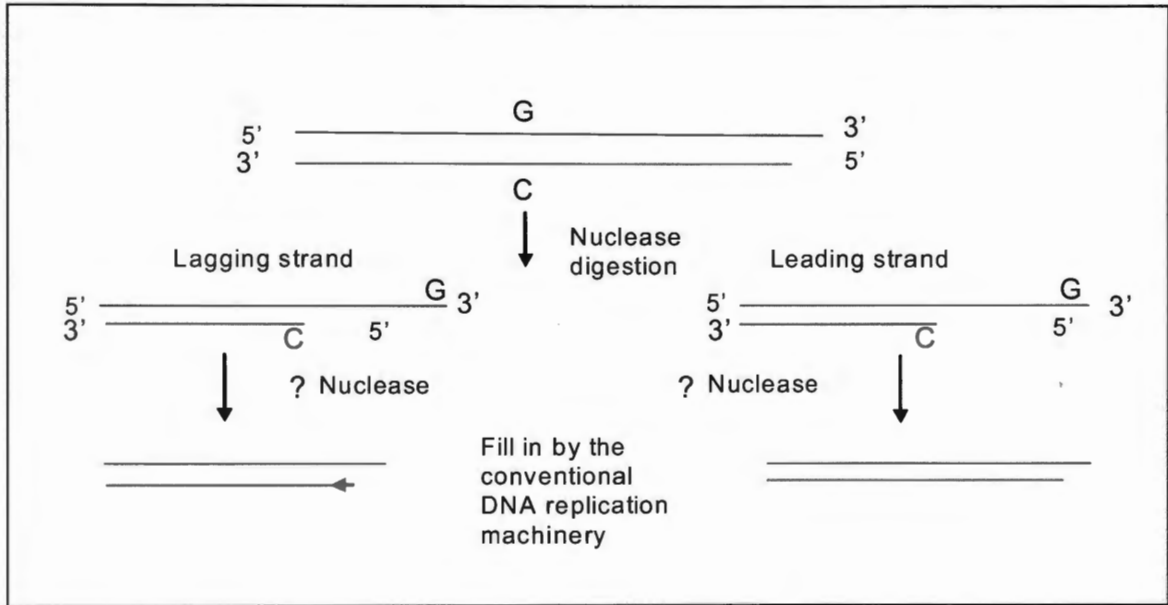
Figure 18. Alternative mechanism for G-overhang generation in human cells. Long overhangs could be generated in the late S phase of the cell cycle due to extensive nuclease (unknown) digestion on both the strands and these could be later filled in by the conventional DNA replication machinery.

REFERENCES

1. Guo, X., Deng, Y., Lin, Y., Cosme-Blanco, W., Chan, S., He, H., Yuan, G., Brown, E.J. and Chang, S. (2007) Dysfunctional telomeres activate an ATM-ATR-dependent DNA damage response to suppress tumorigenesis. *Embo J*, **26**, 4709-4719.

2. Hector, R.E., Shtofman, R.L., Ray, A., Chen, B.R., Nyun, T., Berkner, K.L. and Runge, K.W. (2007) Tel1p preferentially associates with short telomeres to stimulate their elongation. *Mol Cell*, **27**, 851-858.

3. Denchi, E.L. and de Lange, T. (2007) Protection of telomeres through independent control of ATM and ATR by TRF2 and POT1. *Nature*, **448**, 1068-1071.

4. McClintock, B. (1941) The Stability of Broken Ends of Chromosomes in Zea Mays. *Genetics*, **26**, 234-282.

5. Verdun, R.E. and Karlseder, J. (2006) The DNA damage machinery and homologous recombination pathway act consecutively to protect human telomeres. *Cell*, **127**, 709-720.

6. Feldser, D., Strong, M.A. and Greider, C.W. (2006) Ataxia telangiectasia mutated (Atm) is not required for telomerase-mediated elongation of short telomeres. *Proc Natl Acad Sci U S A*, **103**, 2249-2251.

7. Chai, W., Sfeir, A.J., Hoshiyama, H., Shay, J.W. and Wright, W.E. (2006) The involvement of the Mre11/Rad50/Nbs1 complex in the generation of G-overhangs at human telomeres. *EMBO Rep*, **7**, 225-230.

8. Verdun, R.E., Crabbe, L., Haggblom, C. and Karlseder, J. (2005) Functional human telomeres are recognized as DNA damage in G2 of the cell cycle. *Mol Cell*, **20**, 551-561.

9. de Lange, T. (2005) Shelterin: the protein complex that shapes and safeguards human telomeres. *Genes Dev*, **19**, 2100-2110.

10. Chai, W., Shay, J.W. and Wright, W.E. (2005) Human telomeres maintain their overhang length at senescence. *Mol Cell Biol*, **25**, 2158-2168.

11. Hickson, I., Zhao, Y., Richardson, C.J., Green, S.J., Martin, N.M., Orr, A.I., Reaper, P.M., Jackson, S.P., Curtin, N.J. and Smith, G.C. (2004) Identification and characterization of a novel and specific inhibitor of the ataxia-telangiectasia mutated kinase ATM. *Cancer Res*, **64**, 9152-9159.

12. Kim, S.H., Beausejour, C., Davalos, A.R., Kaminker, P., Heo, S.J. and Campisi, J. (2004) TIN2 mediates functions of TRF2 at human telomeres. *J Biol Chem*, **279**, 43799-43804.

13. Chun, H.H. and Gatti, R.A. (2004) Ataxia-telangiectasia, an evolving phenotype. *DNA Repair (Amst)*, **3**, 1187-1196.

14. Jacob, N.K., Kirk, K.E. and Price, C.M. (2003) Generation of telomeric G strand overhangs involves both G and C strand cleavage. *Mol Cell*, **11**, 1021-1032.

15. Shiloh, Y. (2003) ATM and related protein kinases: safeguarding genome integrity. *Nat Rev Cancer*, **3**, 155-168.

16. Jackson, S.P. (2002) Sensing and repairing DNA double-strand breaks. *Carcinogenesis*, **23**, 687-696.

17. Khanna, K.K., Lavin, M.F., Jackson, S.P. and Mulhern, T.D. (2001) ATM, a central controller of cellular responses to DNA damage. *Cell Death Differ*, **8**, 1052-1065.

18. Kastan, M.B. and Lim, D.S. (2000) The many substrates and functions of ATM. *Nat Rev Mol Cell Biol*, **1**, 179-186.

19. Hemann, M.T. and Greider, C.W. (1999) G-strand overhangs on telomeres in telomerase-deficient mouse cells. *Nucleic Acids Res*, **27**, 3964-3969.

20. Griffith, J.D., Comeau, L., Rosenfield, S., Stansel, R.M., Bianchi, A., Moss, H. and de Lange, T. (1999) Mammalian telomeres end in a large duplex loop. *Cell*, **97**, 503-514.

21. Blasco, M.A., Lee, H.W., Hande, M.P., Samper, E., Lansdorp, P.M., DePinho, R.A. and Greider, C.W. (1997) Telomere shortening and tumor formation by mouse cells lacking telomerase RNA. *Cell*, **91**, 25-34.

22. Makarov, V.L., Hirose, Y. and Langmore, J.P. (1997) Long G tails at both ends of human chromosomes suggest a C strand degradation mechanism for telomere shortening. *Cell*, **88**, 657-666.

23. Dionne, I. and Wellinger, R.J. (1996) Cell cycle-regulated generation of single-stranded G-rich DNA in the absence of telomerase. *Proc Natl Acad Sci U S A*, **93**, 13902-13907.

24. Lin, J.J. and Zakian, V.A. (1996) The Saccharomyces CDC13 protein is a single-strand TG1-3 telomeric DNA-binding protein in vitro that affects telomere behavior in vivo. *Proc Natl Acad Sci U S A*, **93**, 13760-13765.

25. Wellinger, R.J., Ethier, K., Labrecque, P. and Zakian, V.A. (1996) Evidence for a new step in telomere maintenance. *Cell*, **85**, 423-433.

26. Savitsky, K., Sfez, S., Tagle, D.A., Ziv, Y., Sartiel, A., Collins, F.S., Shiloh, Y. and Rotman, G. (1995) The complete sequence of the coding region of the ATM gene reveals similarity to cell cycle regulators in different species. *Hum Mol Genet*, **4**, 2025-2032.

27. Makarov, V.L., Lejnine, S., Bedoyan, J. and Langmore, J.P. (1993) Nucleosomal organization of telomere-specific chromatin in rat. *Cell*, **73**, 775-787.

28. Olovnikov, A.M. (1973) A theory of marginotomy. The incomplete copying of template margin in enzymic synthesis of polynucleotides and biological significance of the phenomenon. *J Theor Biol*, **41**, 181-190.

29. Watson, J.D. (1972) Origin of concatemeric T7 DNA. *Nat New Biol*, **239**, 197-201.

30. Greider, C.W. and Blackburn, E.H. (1985) Identification of a specific telomere terminal transferase activity in Tetrahymena extracts. *Cell*, **43**, 405-413.

31.   Henderson, E., Hardin, C.C., Walk, S.K., Tinoco, I., Jr. and Blackburn, E.H. (1987) Telomeric DNA oligonucleotides form novel intramolecular structures containing guanine-guanine base pairs. *Cell*, **51**, 899-908.

32.   Gatti, R.A., Berkel, I., Boder, E., Braedt, G., Charmley, P., Concannon, P., Ersoy, F., Foroud, T., Jaspers, N.G., Lange, K. *et al.* (1988) Localization of an ataxia-telangiectasia gene to chromosome 11q22-23. *Nature*, **336**, 577-580.

33.   Cooke, H.J. and Smith, B.A. (1986) Variability at the telomeres of the human X/Y pseudoautosomal region. *Cold Spring Harb Symp Quant Biol*, **51 Pt 1**, 213-219.

34.   Allshire, R.C., Gosden, J.R., Cross, S.H., Cranston, G., Rout, D., Sugawara, N., Szostak, J.W., Fantes, P.A. and Hastie, N.D. (1988) Telomeric repeat from T. thermophila cross hybridizes with human telomeres. *Nature*, **332**, 656-659.

35.   Allshire, R.C., Dempster, M. and Hastie, N.D. (1989) Human telomeres contain at least three types of G-rich repeat distributed non-randomly. *Nucleic Acids Res*, **17**, 4611-4627.

36.   de Lange, T., Shiue, L., Myers, R.M., Cox, D.R., Naylor, S.L., Killery, A.M. and Varmus, H.E. (1990) Structure and variability of human chromosome ends. *Mol Cell Biol*, **10**, 518-527.

37.   Kipling, D. and Cooke, H.J. (1990) Hypervariable ultra-long telomeres in mice. *Nature*, **347**, 400-402.

38. Ray, A. and Runge, K.W. (1999) The yeast telomere length counting machinery is sensitive to sequences at the telomere-nontelomere junction. *Mol. Cell. Biol*, **19**, 31-45.

39. Kim, N.W., Piatyszek, M.A., Prowse, K.R., Harley, C.B., West, M.D., Coviello, G.M., Wright, W.E, Weinrich, S.L. and Shay, J.W. (1994) Specific association of human telomerase activity with immortal cells and cancer. *Science*, **266**, 2011-2015.

40. Dionne, I. and Wellinger, R.J. (1998) Processing of telomeric DNA ends requires the passage of a replication fork. *Nucleic Acids Res*, **26**, 5365-5371.

41. Loayza, D. and de Lange, T. (2004) Telomerase regulation at the telomeres: a binary switch. *Cell,* **117**, 279-280.

42. Myers, J.S. and Cortez, D (2006) Rapid activation of ATR by ionizing radiation requires ATM and Mre11. *J Biol Chem*, **281**, 9346-9350

APPENDIX

Abbreviations

Abbreviations

A-T	Ataxia-Telangiectasia
ATM	Ataxia -Telangiectasia Mutated
ATR	Ataxia Telangiectasia and rad 3-Related
DDR	DNA Damage Response
DMSO	Dimethyl sulphoxide
ds	Double Stranded
ExoI	ExonucleaseI
FACS	Fluorescence Activated Cell Sorting
FAT	Focal Adhesion Targeting
γ-H2AX	Phosphorylated form of histone H2AX
HEAT	Huntington, Elongation Factor 3, PR65/A, TOR
hTR	human Telomerase RNA
hTERT	human Telomerase Reverse Transcriptase
MRN	Mre11-Rad50-Nbs1
NHEJ	Non Homologous End Joining
NLS	Nuclear Localization Signal
PI3K	Phosphotidyl Inositol 3 Kinase
PI3KK	Phosphotidyl Inositol 3 Kinsae like kinase
POT1	Protection of Telomere 1

Rifl	RAP1 interacting factor 1
Rif2	RAP1 interacting factor 2
ss	Single Stranded
TIN2	TRF1- interacting protein 2
TPP1	TIN2 interacting protein 1
TRF1	Telomere Repeat binding Factor 1
TRF2	Telomere Repeat binding Factor 2